

# Geophysical Research Letters

## RESEARCH LETTER

10.1029/2018GL081034

**Key Points:**

- Large-eddy simulation is used to examine the atmospheric response to idealized submesoscale ocean fronts
- Sharp ocean fronts can generate large vertical vorticity and secondary circulation in the atmosphere
- The length scale of the atmospheric response is set by boundary layer dynamics, not just by horizontal turbulent mixing

**Supporting Information:**

- Supporting Information S1

**Correspondence to:**

J.O. Wenegrat,  
jwenegrat@stanford.edu

**Citation:**

Wenegrat, J. O., & Arthur, R. S. (2018). Response of the atmospheric boundary layer to submesoscale sea surface temperature fronts. *Geophysical Research Letters*, 45. <https://doi.org/10.1029/2018GL081034>

Received 22 OCT 2018

Accepted 3 DEC 2018

Accepted article online 6 DEC 2018

## Response of the Atmospheric Boundary Layer to Submesoscale Sea Surface Temperature Fronts

**J. O. Wenegrat<sup>1</sup>  and R. S. Arthur<sup>2</sup> **

<sup>1</sup>Department of Earth System Science, Stanford University, Stanford, CA, USA, <sup>2</sup>Lawrence Livermore National Laboratory, Livermore, CA, USA

**Abstract** Submesoscale sea surface temperature fronts are ubiquitous throughout much of the global ocean; however, the response of the marine atmospheric boundary layer (MABL) to the ocean submesoscale is not well understood. In this manuscript large-eddy simulation is used to explore the time-dependent response of the MABL to idealized submesoscale sea surface temperature fronts, with an emphasis on how the dynamics of the MABL determine the strength and position of gradients in wind speed and air temperature. Results suggest that horizontal mixing only becomes important in response to frontogenesis by horizontally convergent ageostrophic flows, contrary to the common assumption that the MABL response will be strongly dependent on horizontal turbulent mixing. The fronts that develop in the MABL are also associated with large vertical relative vorticity, suggesting the possibility that submesoscale fronts may induce inertial instability in the MABL. These results provide guidance for high-resolution ocean and atmosphere modeling and for interpreting observations.

**Plain Language Summary** The atmosphere responds to changes in sea surface temperature in a variety of important ways; however, it is not currently well understood how the atmosphere responds when the sea surface temperature changes rapidly over small spatial scales. In this article we use very high resolution simulation to explore the response of the atmosphere to idealized small-scale variations in sea surface temperature. The atmospheric temperature and velocity fields are shown to respond quickly to these small-scale ocean temperature gradients. Importantly, the strength and location of the atmospheric response depends on the flow in the atmosphere, contrary to a common assumption that turbulent mixing will dominate the response. The simulation also suggests that the atmosphere might in some cases respond with a growing instability over these ocean fronts. These results provide guidance for high-resolution ocean and atmosphere modeling and for interpreting observations.

### 1. Introduction

An important mechanism for air-sea coupling arises from the sensitivity of the marine atmospheric boundary layer (MABL) to changes in sea surface temperature (SST). Local changes in SST, for example, at ocean fronts and eddies, modify both the dynamic and thermodynamic structure of the MABL, which in turn modifies the surface heat flux and wind stress (Small et al., 2008). These changes in surface fluxes can then feedback on the evolution of the ocean boundary layer, thereby coupling the ocean and atmosphere. This type of air-sea coupling has been demonstrated to be important for a range of ocean and atmosphere processes, including the location and intensity of storms (Chelton & Xie, 2010), energetics of the ocean mesoscale eddy field (Byrne et al., 2016), and the large-scale ocean circulation (Hogg et al., 2009).

Much of our understanding of the physics of how changes in SST couples the atmosphere and ocean comes from considering SST anomalies with horizontal scales of  $O(100 \text{ km})$ , characteristic of the ocean mesoscale (Chelton & Xie, 2010). The focus on air-sea interaction at these scales is driven in part by the current resolution of large-scale ocean models, the availability of satellite SST and vector winds approaching these scales, as well as evidence that air-sea coupling at these scales is stronger than at larger scales (Bishop et al., 2017). At the same time, an important recent development in the field of oceanography has been the recognition of the global prevalence of submesoscale eddies, fronts, and filaments in (with horizontal scales of  $\sim 0.1\text{--}10 \text{ km}$ ) in the upper ocean (McWilliams, 2016). These submesoscale features have been shown to be critical to the dynamics of the upper ocean (Boccaletti et al., 2007; Wenegrat & McPhaden, 2016), helping to set the global

ocean mixed-layer heat budget (Su et al., 2018) and modifying the interior properties of the ocean gyres (Wenegrat et al., 2018).

Observations and models of the MABL also suggest that submesoscale SST variability modifies the thermal structure and wind field in the MABL (Kudryavtsev et al., 1996; Lambaerts et al., 2013; Perlin et al., 2007; Sweet et al., 1981). However there are a priori reasons to expect that the MABL response to the submesoscale will differ from larger scales, most notably that submesoscale SST features can evolve on fast timescales (hours to days), and that the horizontal length scale of the submesoscale is comparable to the MABL depth. These aspects of the submesoscale invalidate two common assumptions taken to study air-sea interaction at the ocean mesoscale: Steady-state dynamics and small aspect ratio (see Schneider & Qiu, 2015). Thus, despite the focus in the field of oceanography on the submesoscale it remains largely unknown how SST variability at this scale modifies the MABL and, importantly, how this might alter the pathways to air-sea coupling that have been identified at the ocean mesoscale.

In this manuscript we present results from an idealized large-eddy simulation (LES) of the MABL response to wind oriented along submesoscale SST fronts. A particular emphasis is on the dynamical response of the MABL, including how unsteady dynamics modify the response at the submesoscale, and the role of ageostrophic cross-frontal flow in setting the spatial scale and location of the atmospheric response relative to the SST fronts. Our findings suggest that submesoscale SST fronts can rapidly generate significant changes in near-surface winds, and that near-surface frontogenesis allows the MABL to respond at horizontal length scales that are smaller than the full MABL depth. These sharp gradients can be associated with strong signals in both horizontal divergence and vertical relative vorticity, leading to the possibility that submesoscale SST fronts induce inertial instability in the MABL. The results of this work have potential implications for both scientific and applied problems, as high-resolution ocean and atmosphere models are increasingly common tools for both fundamental research and operational purposes. Likewise, understanding the basic dynamical response of the MABL in the idealized setting used here may contribute towards interpreting observations, both in situ and from future remote sensing missions that will begin to resolve these scales.

## 2. Parameter Space and Numerical Simulation

A useful parameter for considering the MABL response to a gradient in SST is (Kilpatrick et al., 2014)

$$\epsilon = \frac{U}{fL^{SST}}, \quad (1)$$

where  $U$  defines a typical scale for the component of the wind aligned parallel, or anti-parallel, to the surface SST gradient ( $\mathbf{u} \cdot \nabla_h \text{SST} / |\nabla_h \text{SST}| \sim U$ ), and  $L^{SST}$  is the length scale over which the SST varies. Using this definition  $\epsilon$  can be understood as a “cross-frontal” Rossby number, defining the ratio of the advective length scale in the atmosphere to the length scale of the SST gradient,  $\epsilon = L^A / L^{SST}$ . Another important parameter is the boundary layer aspect ratio, which we define here as

$$\gamma = \frac{H^{BL}}{L^{SST}}, \quad (2)$$

the ratio of the atmospheric boundary layer depth to the SST length scale.

The dynamical response of the MABL as a function of  $\epsilon$ , in the limit of  $\gamma \ll 1$  appropriate for the ocean mesoscale, is concisely summarized in Schneider & Qiu, (2015 and references therein). Ocean submesoscale fronts though occupy a unique portion of parameter space that has not been well explored. Importantly, the small horizontal length scales of the ocean submesoscale suggest  $\gamma \sim O(1)$ , which is often interpreted to imply that horizontal mixing will play a dominant role in the MABL response. However, the processes responsible for setting the horizontal length scale of boundary layer fronts are not currently well understood, and we will show below that the role of horizontal mixing can depend strongly dependent on the dynamical response of the MABL. In the case of cross-frontal winds it is also clear that  $\epsilon \gg 1$ , regardless of whether the winds are strong or weak. Less obvious is that even in the case of a background wind-field that is aligned along a front, the time-dependent response of the MABL to SST perturbations will also lead to  $\epsilon \geq 1$ , suggesting that the portion of parameter space with  $\epsilon \ll 1$  is not physically relevant for small  $L^{SST}$ .

To explore the MABL response to SST fronts in the portion of parameter space where  $\gamma \sim O(1)$ , we use the Weather Research and Forecasting model (WRF; Skamarock et al., 2008). The computational domain is doubly

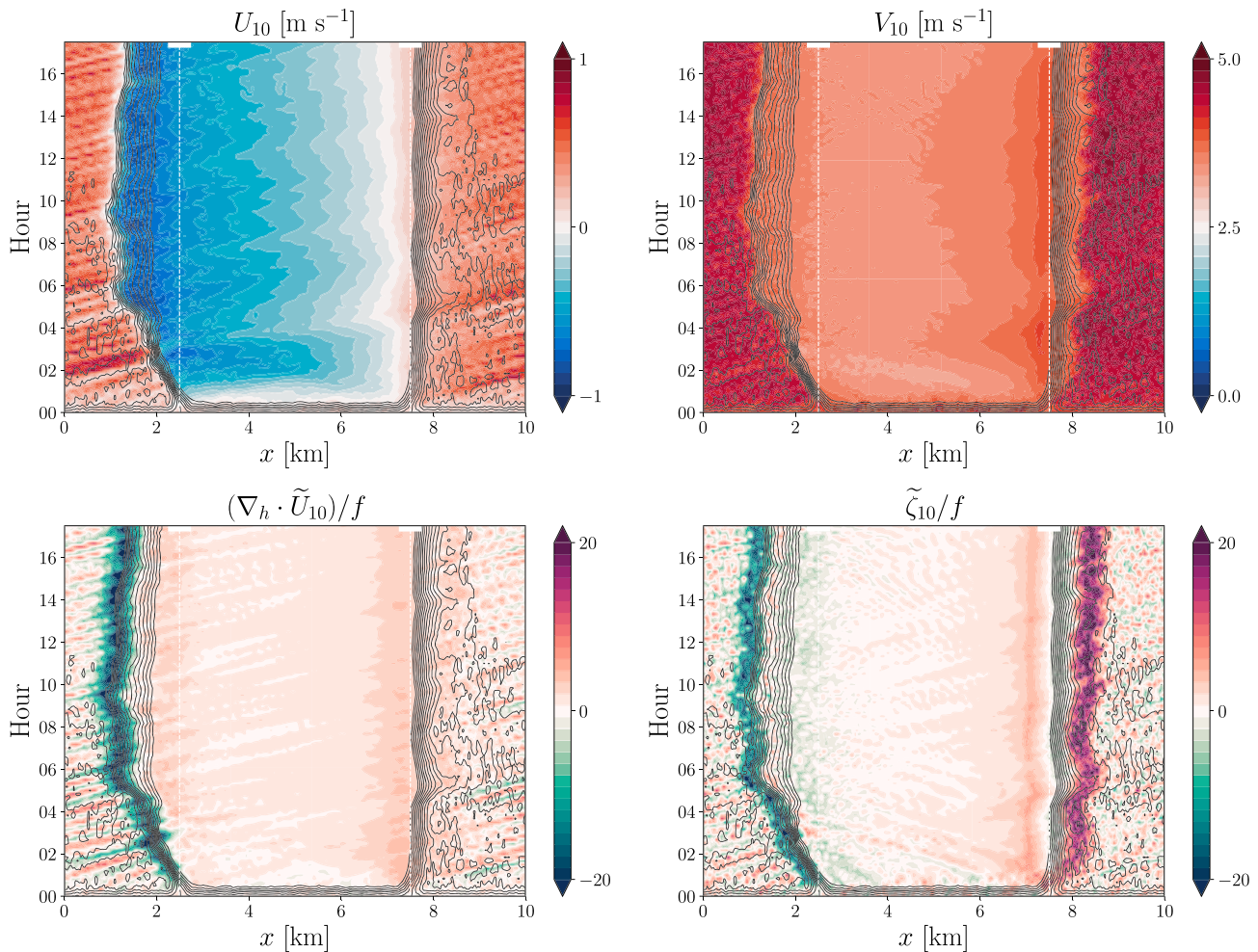


**Figure 1.** Along-front averaged fields at  $z = 10$  m. (top) Across-front velocity ( $U_{10}$ ), and along-front velocity ( $V_{10}$ ). (bottom) Horizontal divergence ( $\nabla_h \cdot \tilde{U}_{10}$ ), and vertical relative vorticity ( $\tilde{\zeta}_{10}$ ), both normalized by the Coriolis frequency. Thin black contours indicate the atmospheric temperature anomaly field with contour intervals of 0.01 K, thick white lines indicate regions of sea surface temperature gradient, and thin dashed-white lines indicate the center of each sea surface temperature front. Divergence and vorticity are smoothed to 500-m horizontal resolution, and temperature is smoothed over 30 min, to reduce noise.

periodic in the horizontal, with domain size  $(L^x, L^y, L^z) = (10, 3, 2)$  km. Surface fluxes are calculated using WRF revised MM5 surface layer formulation (Jiménez et al., 2012) with exchange coefficients based on the COARE 3.0 formula (Fairall et al., 2003). The model is run in an LES configuration ( $\Delta x = \Delta y = 20$  m,  $\Delta z = 5 - 20$  m) and is described in detail in the supporting information.

The simulation begins with a two-inertial period spin-up period, after which an idealized SST field is imposed (Figure S2). A geostrophically balanced background wind of  $|\mathbf{u}_0| = 5$  m/s is held constant throughout the entire simulation (see the supporting information). The initial state of the forced run consists of a MABL height of  $\approx 1$  km, and 10 m winds oriented in the  $y$ -direction, with relaxation of the wind above  $z = 1.5$  km to the initial background wind state. The case of cross-frontal winds was studied by Skillingstad et al. (2007), so here we impose an idealized SST field consisting of two parallel, equidistant, straight-fronts oriented in the  $y$ -direction, with  $L^{SST} = 500$  m (such that  $\gamma = 2$ ). We refer to areas where winds would blow in the same (opposite) direction as the ocean thermal-wind shear as being “downfront” (“upfront”), consistent with the oceanographic literature. The cross-frontal temperature difference is  $\Delta SST = 0.65$  K, representative of a strong submesoscale ocean front with a cross-frontal buoyancy gradient of  $\Delta b/L^{SST} = (16f)^2 s^{-2}$ . A run with a smaller cross-frontal temperature difference of  $\Delta SST = 0.16$  K ( $\Delta b/L^{SST} = (8f)^2 s^{-2}$ ) gave very similar results (see the supporting information).

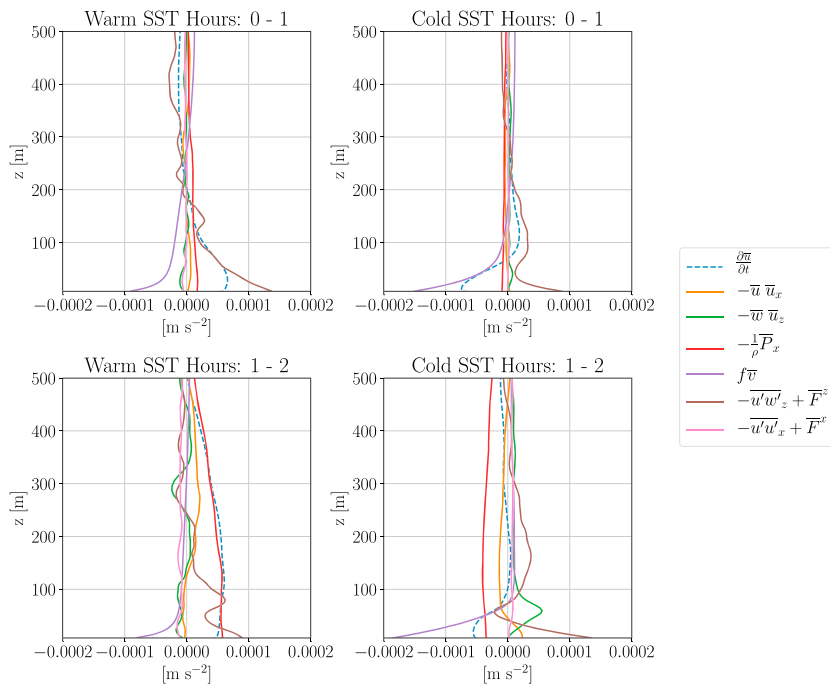


**Figure 2.** Momentum budget terms averaged over the warm sea surface temperature (SST) region away from the marine atmospheric boundary layer fronts ( $x < 1.5$  km and  $x > 8$  km, left column) and cold SST region away from fronts ( $x = 3-7$  km, right column), for hours 0–1 (top row) and hours 1–2 (bottom row). Note that the budgets are plotted as perturbations from the spatially and temporally constant background geostrophically balanced wind field,  $\mathbf{u}_0$ , and hence do not include the background Coriolis and pressure gradient terms. Terms are defined in the legend, with subscripts indicating differentiation, along-front averages indicated by the overbar, and primes indicating departure from the along-front mean. The terms  $F^z$  and  $F^x$  are the subgrid vertical and horizontal stress divergence terms, respectively. SST = sea surface temperature.

### 3. Results

Figure 1 shows an overview of the evolution of the simulation. Over the cold portion of the domain ( $x = 2.5-7.5$  km) the near-surface layer cools rapidly, establishing a stably stratified internal boundary layer. The decrease in turbulent boundary layer height enhances the near-surface turbulent momentum flux divergence, despite a moderate reduction in surface stress, thereby decelerating the near-surface along-front winds (Samelson et al., 2006; Skillingstad et al., 2007; Spall, 2007). In contrast, over the warm portion of the domain ( $x < 2.5$  km and  $x > 7.5$  km) turbulent momentum mixing extends higher into the MABL, decreasing the turbulent momentum flux divergence and allowing an acceleration of the along-front flow. The initial wind-profile used here has very little vertical shear in the upper portion of the boundary layer (Figure S1); hence, vertical mixing of momentum down from aloft does not significantly alter the along-front flow; however, in cases with stronger vertical shear this mechanism may further accelerate near-surface winds over warm SST (Hayes et al., 1989; Wallace et al., 1989). The changes in along-front velocity in this simulation are an order of magnitude larger than predicted by applying observed mesoscale SST-Wind coupling coefficients (O'Neill et al., 2012), which would suggest  $\Delta V \approx 0.4\Delta SST \approx 0.26$  m/s. This may reflect either different physics at these scales, or the temporal and spatial averaging inherent in the formation of the observational estimates. The large change in along-front velocity across the sharp boundary-layer fronts also generates large vertical vorticity, the significance of which is discussed further below.

Changes in the along-front component of the wind and the zonal turbulent stress divergence also act in concert to accelerate across-front flows. Over the cold portion of the domain the initial negative cross-frontal acceleration is generated both by a reduction in the turbulent vertical stress divergence and by the unbalanced portion of the Coriolis acceleration term in the zonal momentum balance, which is negative near the surface (i.e.,  $f\Delta v < 0$ , Figure 2). Over the warm pool the near-surface cross-frontal acceleration is positive, forced by enhanced turbulent stress divergence and the reduced magnitude of the Coriolis acceleration. The resulting cross-frontal flow remains small (with turning of the wind of only  $\sim 10^\circ$  compared to the initial

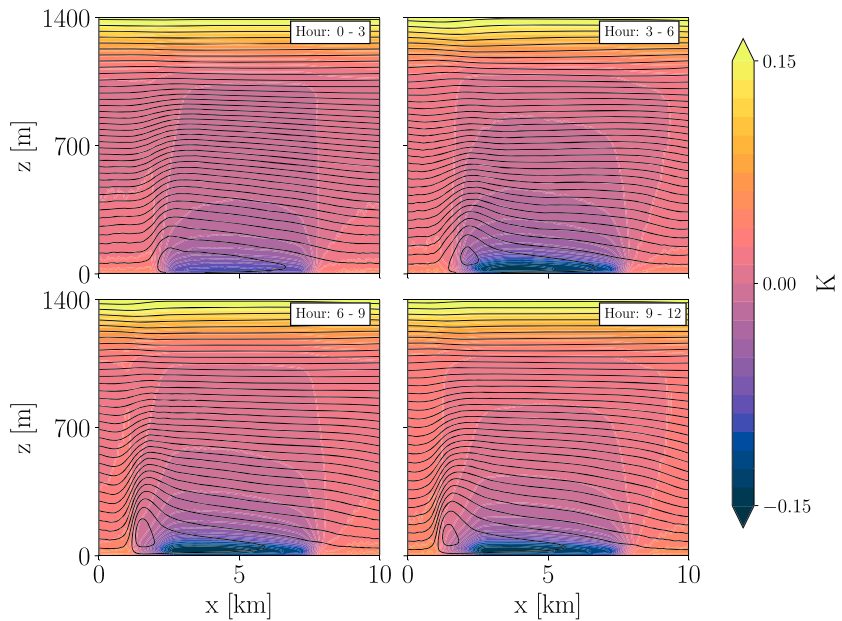


**Figure 3.** Air temperature anomaly (color scale), averaged in the along-front direction and over the time periods indicated, and the overturning stream function  $\Psi$  (black contours), defined such that flow is clockwise around closed contours. The stream function is contoured every  $25 \text{ m}^2/\text{s}$ .

condition); however, given the small length scale of the SST fronts this weak wind still implies a cross-frontal Rossby number of  $\epsilon \sim O(10)$ , suggesting that some of the mechanisms identified for strong cross-frontal winds at the ocean mesoscale (Kilpatrick et al., 2014; Skyllingstad et al., 2007) may remain relevant at the submesoscale regardless of the orientation of the background wind.

This pattern of cross-frontal flow also generates significant horizontal convergence and divergence over the upfront and downfront side of the cold region, respectively (Figure 1). This generates a secondary-circulation in the  $x$ - $z$  plane (Figure 3), with ascending motions on the upfront side of the cold region, and more diffuse descending motions over the cold region (similar to the response observed over larger-scale fronts by Kilpatrick et al., 2016). This secondary circulation is established initially by the cross-frontal winds accelerated through the initial adjustment to the SST field, as discussed above. However, advection of temperature anomalies by the secondary circulation and positive cross-frontal flow above the internal boundary layer generates a pressure-gradient forcing that becomes leading order after approximately an hour of simulation time (Figure 2, bottom). The pressure-gradient accelerations are of the same sign as the initial cross-frontal accelerations; hence, they reinforce the near-surface flow and secondary circulation, which continues to strengthen and extend through the MABL (Figure 3). Nonlinear effects further modify the momentum balance, for instance, vertical advection by the descending branch of the secondary circulation generates a positive cross-frontal acceleration near the top of the internal boundary layer (Figure 2, bottom right). The effects of the secondary circulation also extend into the inversion layer, particularly over the ascending branch, where  $w \sim O(1 \text{ cm/s})$  at  $z = 1,100 \text{ m}$  after 2 hr of simulation time, suggesting the possibility of a free-atmosphere response to submesoscale SST variability.

The secondary circulation has important implications for how the horizontal length scale of the MABL response to submesoscale SST fronts is set. For a 2-D front in the  $x$ - $z$  plane the governing equation for temperature frontogenesis can be written as

$$\frac{1}{2} \frac{D|\bar{\theta}_x|^2}{Dt} = \underbrace{-\bar{u}_x |\bar{\theta}_x|^2}_{HCNV} - \underbrace{\bar{w}_x \bar{\theta}_z \bar{\theta}_x}_{VDEF} - \underbrace{-\bar{W}' \bar{\theta}'_{zx} \bar{\theta}_x + \bar{F}_x^z \bar{\theta}_x}_{VMIX} - \underbrace{-\bar{U}' \bar{\theta}'_{xx} \bar{\theta}_x + \bar{F}_x^x \bar{\theta}_x}_{HMIX}, \quad (3)$$

with notation as described in the caption of Figure 2. The Lagrangian rate of change of the temperature gradient is thus a function of horizontal convergence (HCNV), vertical deformation which converts vertical gradients into horizontal gradients (VDEF), and vertical (VMIX) and horizontal (HMIX) mixing by the resolved

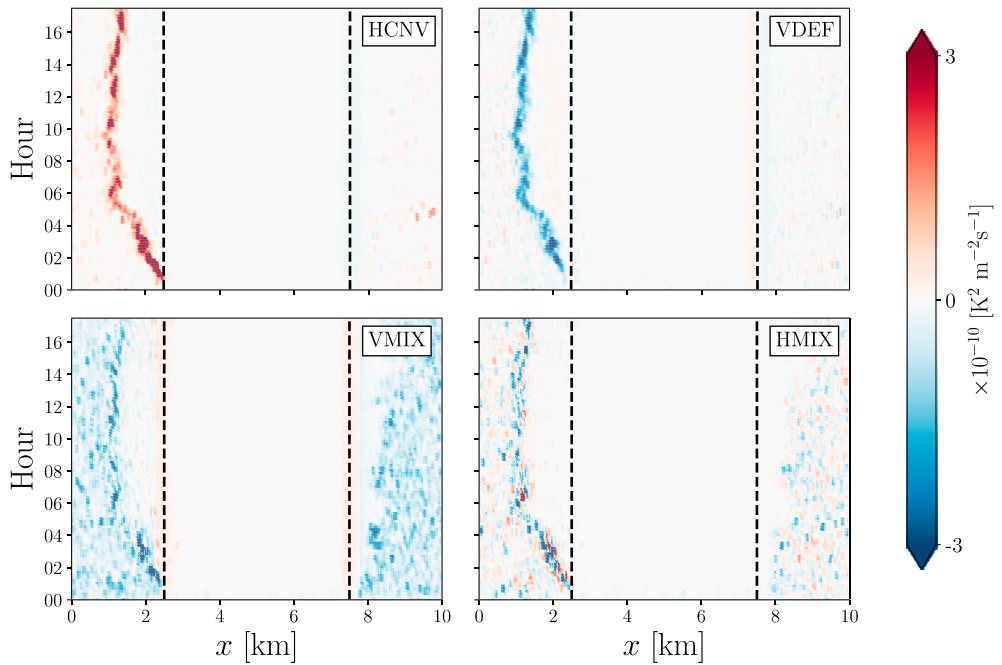


**Figure 4.** Right-hand side terms of the frontogenesis function (equation (3)), at  $z = 10$  m. Fields are smoothed over 100 m in the horizontal and 30 min in time to reduce noise.

and parameterized turbulent motions. The evolution of the right-hand side terms near the surface are shown in Figure 4. The initial temperature gradient generated by the SST front is sharpened on the upfront side of the cold region by the horizontal convergence of the across-front flow, leading to a very sharp near-surface front between hours 1–4 (Figure 1). This frontogenesis is then arrested by a combination of vertical deformation and horizontal and vertical mixing, leading to a quasi-steady temperature field consisting of a sharp front near  $x = 1$  km with a weaker temperature gradient extending from  $x = 1$ –2 km. In contrast, on the downfront side of the cold region all terms in (3) are much weaker, with an approximate balance between frontogenesis by vertical mixing directly over the SST front, and HCNV, which is frontolytic due to the divergent flow associated with the descending branch of the secondary circulation. For both fronts cross-frontal advection shifts the location of maximum  $|\theta_x|$  away from the surface SST gradients. Similar results are also found for temperature frontogenesis higher in the MABL, and for the velocity frontogenesis function (not shown here). The dynamics of the MABL thus play a leading order role in setting the strength and location of the gradients in MABL temperature and velocity in response to an SST front, even for  $\gamma \sim 1$ , where it is often assumed the response will be a balance between surface forcing (through VMIX) and horizontal mixing (HMIX). The implications of these findings are discussed in section 4.

An important consequence of the strong modification of the along-front velocity by the change in SST is the development of strong vertical relative vorticity in the boundary layer (Figure 1), which can modify Ekman dynamics (Wenegrat & Thomas, 2017). These vorticity signals develop on a timescale set by the initial adjustment of the along-front flow to the changes in vertical mixing, leading to  $|\zeta_{10}| \gg |f|$  after approximately 1 hr. On the downfront side the vertical vorticity is positive, which can modify the frequency and energetics of inertial oscillations in the boundary layer (Whitt & Thomas, 2015). On the upfront side of the domain the vertical vorticity is strongly negative, such that  $f + \zeta_{10} < 0$  (Figure 1), a state that is linearly unstable to growing inertial instability (Emanuel, 1979; Hoskins, 1974). This suggests the possibility that upfront winds over submesoscale SST fronts could become inertially unstable. These instabilities extract energy from the mean flow and, importantly, generate secondary instabilities that enhance boundary layer turbulence (which in a more physically realistic context might occur either locally or downwind of the SST front; Jiao & Dewar, 2015). Future work will consider the potential implications of this mechanism for the evolution of the MABL and air-sea coupling at these scales.

#### 4. Conclusions

In this manuscript we described a LES of the MABL response to an idealized submesoscale SST field, which shows that winds blowing along sharp SST fronts are rapidly modified by changes in the vertical turbulent stress divergence. This generates unbalanced accelerations in the across-front momentum balance, creating cross-frontal flows that, while weak in absolute value, still imply large cross-frontal Rossby numbers ( $\epsilon \gg 1$ ). Convergence of cross-frontal flows force secondary circulations which help generate temperature and pressure gradients that are of the sense to enhance the cross-frontal secondary circulation. These ageostrophic flows set both the strength and the location of the MABL temperature and velocity gradients through frontogenesis and horizontal advection, providing a counter-example to the common assumption that horizontal mixing will dominate when the boundary layer aspect ratio is not small ( $\gamma \sim O(1)$ ). Finally, the sharp fronts that develop in the MABL are associated with large magnitude vertical relative vorticity, suggesting the possibility that sharp SST fronts could induce inertial instability in the MABL.

The model setup used here is highly idealized, with two closely spaced SST fronts in a doubly periodic domain. This limitation reflects the computational demands of LES modeling; however, the results still provide useful guidance for understanding the MABL response to more physically realistic configurations. For example, the analysis here suggests that similar dynamics (i.e., unbalanced changes in along-front momentum accelerating a secondary-circulation in the across-front direction) could arise at an isolated submesoscale front, with parallels to a sea-breeze circulation (Miller, 2003), consistent with observations along the Gulf Stream front (Sweet et al., 1981). Further, assuming that air-parcels are advected by the mean along-front wind speed, an hour of simulation time here can be considered as representing approximately 15 km of along-front distance. Many submesoscale features have along-front length scales exceeding this, for instance, Gula et al. (2014) discuss cold filaments in a realistic model of the Gulf Stream region with along-front lengths exceeding 60 km. Likewise many large-scale ocean fronts such as the Gulf Stream, Kuroshio, and equatorial cold-tongue front, have embedded sharp fronts where  $\gamma \sim O(1)$  (D'Asaro et al., 2011; Thomas et al., 2016; Warner et al., 2018). The major aspects of the MABL response in our simulation are established within approximately 1–2 hr of simulation time, suggesting similar dynamics may be at play in the real atmosphere.

The results presented here provide guidance for interpreting observations and for high-resolution ocean and atmosphere modeling. For instance, it is common practice when running coupled ocean-atmosphere models to run the atmosphere component at lower resolution than the ocean component. This is sometimes justified in light of the relative boundary layer aspect ratios of the two fluids; however, our results suggest that boundary layer frontogenesis can allow the MABL to respond at a length scale comparable to that of a submesoscale front. Horizontal mixing serves to arrest frontogenesis but does not independently constrain the scale of the atmospheric response, contrary to expectations based on scaling the Reynolds-averaged equations of motion. Lack of correlation between changes in SST and the MABL response at these scales in lower-resolution models could be a consequence of the models being overly diffusive in the horizontal, or advective effects which shift the MABL gradients relative to SST (Figure 1, Lambaerts et al., 2013; Spall, 2007). Further, the strong vorticity signal that develops in the atmospheric boundary layer suggests that the MABL response to upfront and downfront winds may not be symmetric, with upfront winds potentially leading to inertially unstable conditions. Future work should consider more realistic SST configurations, as well as the transition between the along-front wind case considered here and the across-front wind case considered in Skillingstad et al. (2007). Such studies will be important for improving high-resolution atmosphere and ocean models and for guiding the interpretation of data from future remote sensing missions that will begin to resolve the ocean submesoscale.

#### Acknowledgments

Model configuration files are available at <http://github.com/wenegrat/WenegratArthur>, and all model output used in this analysis is available by request. J. O. W. was supported by NSF grant OCE-1459677. A portion of this work was prepared by LLNL under contract DE-AC52-07NA27344. The authors thank two anonymous reviewers for their comments, as well as NSF for the opportunity to attend PODS IX, where this collaboration was initiated.

#### References

- Bishop, S. P., Small, R. J., Bryan, F. O., & Tomas, R. A. (2017). Scale dependence of midlatitude air-sea interaction. *Journal of Climate*, 30(20), 8207–8221. <https://doi.org/10.1175/JCLI-D-17-0159.1>
- Boccaletti, G., Ferrari, R., & Fox-Kemper, B. (2007). Mixed layer instabilities and restratification. *Journal of Physical Oceanography*, 37(9), 2228–2250. <https://doi.org/10.1175/JPO3101.1>
- Byrne, D., Münnich, M., Frenger, I., & Gruber, N. (2016). Mesoscale atmosphere ocean coupling enhances the transfer of wind energy into the ocean. *Nature Communications*, 7. <https://doi.org/10.1038/ncomms11867>
- Chelton, D., & Xie, S.-P. (2010). Coupled ocean-atmosphere interaction at oceanic mesoscales. *Oceanography*, 23(4), 52–69. <https://doi.org/10.5670/oceanog.2010.05>
- D'Asaro, E., Lee, C., Rainville, L., Harcourt, R., & Thomas, L. (2011). Enhanced turbulence and energy dissipation at ocean fronts. *Science*, 332(6027), 318–322. <https://doi.org/10.1126/science.1201515>

- Emanuel, K. A. (1979). Inertial instability and mesoscale convective systems. Part I: Linear theory of inertial instability in rotating viscous fluids. *Journal of the Atmospheric Sciences*, 36(12), 2425–2449. [https://doi.org/10.1175/1520-0469\(1979\)036<2425:IIAMCS>2.0.CO;2](https://doi.org/10.1175/1520-0469(1979)036<2425:IIAMCS>2.0.CO;2)
- Fairall, C. W., Bradley, E. F., Hare, J. E., Grachev, A. A., & Edson, J. B. (2003). Bulk parameterization of air-sea fluxes: Updates and verification for the COARE algorithm. *Journal of Climate*, 16(4), 571–591. [https://doi.org/10.1175/1520-0442\(2003\)016<0571:BPOASF>2.0.CO;2](https://doi.org/10.1175/1520-0442(2003)016<0571:BPOASF>2.0.CO;2)
- Gula, J., Molemaker, M. J., & McWilliams, J. C. (2014). Submesoscale cold filaments in the Gulf Stream. *Journal of Physical Oceanography*, 44(10), 2617–2643. <https://doi.org/10.1175/JPO-D-14-0029.1>
- Hayes, S. P., McPhaden, M. J., & Wallace, J. M. (1989). The influence of sea-surface temperature on surface wind in the eastern equatorial Pacific: Weekly to monthly variability. *Journal of Climate*, 2(12), 1500–1506. [https://doi.org/10.1175/1520-0442\(1989\)002<1500:TIOSST>2.0.CO;2](https://doi.org/10.1175/1520-0442(1989)002<1500:TIOSST>2.0.CO;2)
- Hogg, A. M. C., Dewar, W. K., Berloff, P., Kravtsov, S., & Hutchinson, D. K. (2009). The effects of mesoscale ocean-atmosphere coupling on the large-scale ocean circulation. *Journal of Climate*, 22(15), 4066–4082. <https://doi.org/10.1175/2009JCLI2629.1>
- Hoskins, B. J. (1974). The role of potential vorticity in symmetric stability and instability. *Quarterly Journal of the Royal Meteorological Society*, 100(425), 480–482. <https://doi.org/10.1002/qj.49710042520>
- Jiao, Y., & Dewar, W. K. (2015). The energetics of centrifugal instability. *Journal of Physical Oceanography*, 45(6), 1554–1573. <https://doi.org/10.1175/JPO-D-14-0064.1>
- Jiménez, P. A., Dudhia, J., González-Rouco, J. F., Navarro, J., Montávez, J. P., & García-Bustamante, E. (2012). A revised scheme for the WRF surface layer formulation. *Monthly Weather Review*, 140(3), 898–918. <https://doi.org/10.1175/MWR-D-11-00056.1>
- Kilpatrick, T., Schneider, N., & Qiu, B. (2014). Boundary layer convergence induced by strong winds across a midlatitude SST front. *Journal of Climate*, 27(4), 1698–1718. <https://doi.org/10.1175/JCLI-D-13-00101.1>
- Kilpatrick, T., Schneider, N., & Qiu, B. (2016). Atmospheric response to a midlatitude SST front: Alongfront winds. *Journal of the Atmospheric Sciences*, 73(9), 3489–3509. <https://doi.org/10.1175/JAS-D-15-0312.1>
- Kudryavtsev, V. N., Grodsky, S. A., Dulov, V. A., & Malinovsky, V. V. (1996). Observations of atmospheric boundary layer evolution above the Gulf Stream frontal zone. *Boundary-Layer Meteorology*, 79(1-2), 51–82. <https://doi.org/10.1007/BF00120075>
- Lambaerts, J., Lapeyre, G., Plougouen, R., & Klein, P. (2013). Atmospheric response to sea surface temperature mesoscale structures. *Journal of Geophysical Research: Atmospheres*, 118, 9611–9621. <https://doi.org/10.1002/jgrd.50769>
- McWilliams, J. C. (2016). Submesoscales current in the ocean. *Proceedings of the Royal Society A: Mathematical, Physical and Engineering Science*, 472(2189), 20160117. <https://doi.org/10.1098/rspa.2016.0117>
- Miller, S. T. K. (2003). Sea breeze: Structure, forecasting, and impacts. *Reviews of Geophysics*, 41(3), 1011. <https://doi.org/10.1029/2003RG000124>
- O'Neill, L. W., Chelton, D. B., & Esbensen, S. K. (2012). Covariability of surface wind and stress responses to sea surface temperature fronts. *Journal of Climate*, 25(17), 5916–5942. <https://doi.org/10.1175/JCLI-D-11-00230.1>
- Perlin, N., Skillingstad, E. D., Samelson, R. M., & Barbour, P. L. (2007). Numerical simulation of air-sea coupling during coastal upwelling. *Journal of Physical Oceanography*, 37(8), 2081–2093. <https://doi.org/10.1175/JPO3104.1>
- Samelson, R. M., Skillingstad, E. D., Chelton, D. B., Esbensen, S. K., O'Neill, L. W., & Thun, N. (2006). On the coupling of wind stress and sea surface temperature. *Journal of Climate*, 19(8), 1557–1566. <https://doi.org/10.1175/JCLI3682.1>
- Schneider, N., & Qiu, B. (2015). The atmospheric response to weak sea surface temperature fronts. *Journal of the Atmospheric Sciences*, 72(9), 3356–3377. <https://doi.org/10.1175/JAS-D-14-0212.1>
- Skamarock, W. C., Klemp, J. B., Dudhia, J., Gill, D. O., Barker, D. M., Wang, W., & Powers, J. G. (2008). A description of the Advanced Research WRF version 3. (*NCAR Technical note -475+STR*). Boulder, Colorado: National Center for Atmospheric Research.
- Skillingstad, E. D., Vickers, D., Mahrt, L., & Samelson, R. (2007). Effects of mesoscale sea-surface temperature fronts on the marine atmospheric boundary layer. *Boundary-Layer Meteorology*, 123(2), 219–237. <https://doi.org/10.1007/s10546-006-9127-8>
- Small, R. J., deSzoeke, S. P., Xie, S. P., O'Neill, L., Seo, H., Song, Q., et al. (2008). Air-sea interaction over ocean fronts and eddies. *Dynamics of Atmospheres and Oceans*, 45(3-4), 274–319. <https://doi.org/10.1016/j.dynatmoce.2008.01.001>
- Spall, M. A. (2007). Midlatitude wind stress-sea surface temperature coupling in the vicinity of oceanic fronts. *Journal of Climate*, 20(15), 3785–3801. <https://doi.org/10.1175/JCLI4234.1>
- Su, Z., Wang, J., Klein, P., Thompson, A. F., & Menemenlis, D. (2018). Ocean submesoscales as a key component of the global heat budget. *Nature Communications*, 9(1), 775. <https://doi.org/10.1038/s41467-018-02983-w>
- Sweet, W., Fett, R., Kerling, J., & La Violette, P. (1981). Air-sea interaction effects in the lower troposphere across the north wall of the Gulf Stream. *Monthly Weather Review*, 109(5), 1042–1052. [https://doi.org/10.1175/1520-0493\(1981\)109<1042:ASIEIT>2.0.CO;2](https://doi.org/10.1175/1520-0493(1981)109<1042:ASIEIT>2.0.CO;2)
- Thomas, L. N., Taylor, J. R., D'Asaro, E. A., Lee, C. M., Klymak, J. M., & Shcherbina, A. (2016). Symmetric instability, inertial oscillations, and turbulence at the Gulf Stream front. *Journal of Physical Oceanography*, 46(1), 197–217. <https://doi.org/10.1175/JPO-D-15-0008.1>
- Wallace, J. M., Mitchell, T. P., & Deser, C. (1989). The influence of sea-surface temperature on surface wind in the eastern equatorial Pacific: Seasonal and interannual variability. *Journal of Climate*, 2(12), 1492–1499. [https://doi.org/10.1175/1520-0442\(1989\)002<1492:TIOSST>2.0.CO;2](https://doi.org/10.1175/1520-0442(1989)002<1492:TIOSST>2.0.CO;2)
- Warner, S. J., Holmes, R. M., Hawkins, E. H. M., Hoecker-Martínez, M. S., Savage, A. C., & Moum, J. N. (2018). Buoyant gravity currents released from tropical instability waves. *Journal of Physical Oceanography*, 48(2), 361–382. <https://doi.org/10.1175/JPO-D-17-0144.1>
- Wenegrat, J. O., & McPhaden, M. J. (2016). Wind, waves, and fronts: Frictional effects in a generalized Ekman model. *Journal of Physical Oceanography*, 46(2), 371–394. <https://doi.org/10.1175/JPO-D-15-0162.1>
- Wenegrat, J. O., & Thomas, L. N. (2017). Ekman transport in balanced currents with curvature. *Journal of Physical Oceanography*, 47(5), 1189–1203. <https://doi.org/10.1175/JPO-D-16-0239.1>
- Wenegrat, J. O., Thomas, L. N., Gula, J., & McWilliams, J. C. (2018). Effects of the submesoscale on the potential vorticity budget of ocean mode waters. *Journal of Physical Oceanography*, 48(9), 2141–2165. <https://doi.org/10.1175/JPO-D-17-0219.1>
- Whitt, D. B., & Thomas, L. N. (2015). Resonant generation and energetics of wind-forced near-inertial motions in a geostrophic flow. *Journal of Physical Oceanography*, 45(1), 181–208. <https://doi.org/10.1175/JPO-D-14-0168.1>